Lamellar Structure and Properties in Poly(ethylene terephthalate) Fibers

N. S. MURTHY,[1] D. T. GRUBB,[2] K. ZERO,[1] C. J. NELSON,[3] G. CHEN[3]

[1]AlliedSignal Inc., Research and Technology, P.O. Box 1021, Morristown, New Jersey 07962, USA

[2]Department of Materials Science and Engineering, Cornell University, Ithaca, New York 14853, USA

[3]AlliedSignal, Inc., Fibers Division, Technical Center, Petersburg, Virginia 23804, USA

Received 12 January 1998; accepted 9 May 1998

ABSTRACT: The fibrillar and the lamellar structures in a range of poly(ethylene terephthalate) fibers were studied by small-angle X-ray scattering. The intensity maxima in the lamellar peaks lie on a curve that can be described as an ellipse. Therefore, the two-dimensional images were analyzed in elliptical coordinates. The dimensions of the coherently diffracting lamellar stack, the dimensions of the fibrils, the interfibrillar spacing, and the orientation of the lamellar surfaces were measured in addition to the lamellar spacing. The orientation of the lamellar planes and the size of the lamellar stacks had a better correlation with mechanical properties of the fibers than did the lamellar spacing. In particular, longer and wider lamellar stacks reduced fiber shrinkage, as did the closer alignment of the lamellar normal to the fiber axis. These structural features were also associated with lower tenacity. © 1998 John Wiley & Sons, Inc. J Appl Polym Sci 70: 2527–2538, 1998

Key words: PET fiber; SAXS; lamellar structure; properties

INTRODUCTION

A long sought-after goal in fiber research has been the determination of quantitative structure–property relationships for predicting the performance of fibers. This is not straightforward, because the influences of the various aspects of the structure cannot be studied independently.[1] Wide-angle X-ray investigations have shown that amorphous orientation has a larger influence on the fiber properties than crystallinity and crystal orientation.[2–5] The factors that affect the amorphous orientation also influence structural features on the longer distance scale (~ 1 nm to 0.1 μm) that can be characterized by small-angle X-ray scattering (SAXS).[6] For example, smaller lamellar spacing at a given crystallinity could indicate smaller crystallites that are closer together and smaller amorphous domains; the size of the lamellae and the tilt of the lamellar plane affect the constraints on the amorphous chain segments and thus influence the mechanical properties, such as modulus, tenacity, and shrinkage. New techniques enable us to analyze the SAXS patterns in detail and measure parameters, such as size and orientation of the fibrils, and size and orientation of the lamellae within these fibrils. In this article, we will describe the characterization of the lamellar and fibrillar structure of a fiber, and seek empirical correlation between any of these parameters and the measured physical properties, such as dimensional stability, tenacity, elongation, and modulus in poly(ethylene terephthalate) fibers.

Correspondence to: N. S. Murthy.

Journal of Applied Polymer Science, Vol. 70, 2527–2538 (1998)
 CCC 0021-8995/98/122527-12

EXPERIMENTAL

Four fibers labeled S, T1, T2, and T3 were used in this work. S is drawn from an essentially amorphous, unoriented precursor yarn spun at low speeds. Fibers T1, T2, and T3 are drawn to different ratios (T3 < T2 < T1 < S) from partially oriented yarns spun at higher speeds (T3 > T2 > T1 > S), and these precursor yarns had, respectively, very little, some, and high crystallinity. Fiber S has an intrinsic viscosity (IV) of 0.88, and the T fibers have an IV of 0.91. These IVs were measured in a 60/40 wt % mixture of phenol and tetrachloroethane. S is a conventional high-tenacity fiber, and the others (T series) are dimensionally stable (DSP™) yarns used in applications that require high modulus and low shrinkage. All of the fibers were annealed under constrained (zero stretch and zero relax) conditions at 230°C for 80 s; these annealed fibers are denoted by the label "h."

The fibers were tested mechanically on an Instron 4505 at a strain rate of 0.02 s^{-1}. Ultimate elongation (UE) was calculated as (displacement to break)/(gage length). Initial modulus was calculated as load/(original cross-section) at 5% strain (LASE 5 = load at a specific elongation of 5%). Free shrinkage at 177°C was measured using a Testrite Shrinkage Tester and is given as (change in length/original length) × 100.

The SAXS data were collected on the F1 beamline at the Cornell High Energy Synchrotron Source using a 0.908 Å wavelength radiation detected on a Fuji image plate. The sample-to-detector distance was 743 mm. An area 600 × 600 pixels near the origin was selected and converted into a 300 × 300 pixel (0.2 mm per pixel) image. This image was further converted to a series of one-dimensional scans parallel to the fiber axis (longitudinal slices) at 0.6 mm intervals. A plot of the meridional peak maxima in these scans as a function of S_E (scattering vector parallel to the equator, $s = 2 \sin \theta/\lambda$, where 2θ is the scattering angle and λ is the wavelength of the radiation, and $s = 1/\text{periodicity}$) is between a straight line and a circular arc. This shape could be described as an ellipse whose standard form is[7]

$$(x/a)^2 + (z_0/b)^2 = 1 \quad (1)$$

Let L_M be the periodicity of those lamellae aligned with their normals along the meridian (usually denoted by L as is done later in the text), and L_E is the periodicity of those lamellae aligned with their normals along the equator. If the intensity of the reflection has fallen to 0 before reaching the equator, there may be no such lamellae, and L_E is just an analytical parameter. Using L_M and L_E, eq. (1) can be written as[7]

$$L_\phi^2 = L_M^2 + L_E^2 \tan^2 \phi \quad (2)$$

where ϕ is the angle between the normal to the lamellar plane and the fiber axis (the tilt-angle) angle, and L_ϕ is the lamellar spacing at ϕ in the direction of the fiber axis. Equation (2) describes a straight line whose intercept is L_M^2. The ellipse can be characterized by a ellipticity $\varepsilon = (1 - L_E/L_M)$ or by an extension ratio $R = (L_M^2/L_E^2)^3$.

For further analysis, the entire two-dimensional image was profile-fitted in elliptical coordinates (u-v) to three functions representing the fibrillar/void scattering, lamellar scattering, and the interfibrillar scattering.[8] Parameters that can be calculated from the SAXS data are illustrated in Figure 1. In this model, a fiber is considered to be made of fibrils of diameter D, with an interfibrillar spacing of d. The fibrils are composed of lamellae whose diameter is also assumed to be D. Amorphous chain segments fill the space between the fibrils, as well as between the lamellae within a fibril. L, the long spacing or the lamellar spacing, is the separation between the lamellae along the fiber axis and is usually calculated as the Bragg spacing the lamellar reflection measured along the fiber axis. The angle between the normal to the lamellar surface (also called lamellar surface elsewhere in the article) and the fiber axis is the tilt angle ϕ, and is one-half the azimuthal angular separation between the lamellar reflections in a 4-point pattern; $\phi = 0$ in a true 2-point pattern. The lamellar peak usually arises from a small number (3 or 4) of coherently diffracting lamellae that are in register and scatter as a single entity; this coherence length of the lamellae is designated as h_L, the height of this lamellar stack. The fibril length l_f described previously is equivalent to the dimension of the fibril seen in an electron micrograph. There are usually a few lamellar stacks arranged end-to-end within a fibril.

The long spacing L_M, and the tilt angle ϕ are calculated from the expressions

$$L_M = 2\pi/q_M \quad (3)$$

$$\tan \phi = u \tan v/\sqrt{(u^2 + A^2)} \quad (4)$$

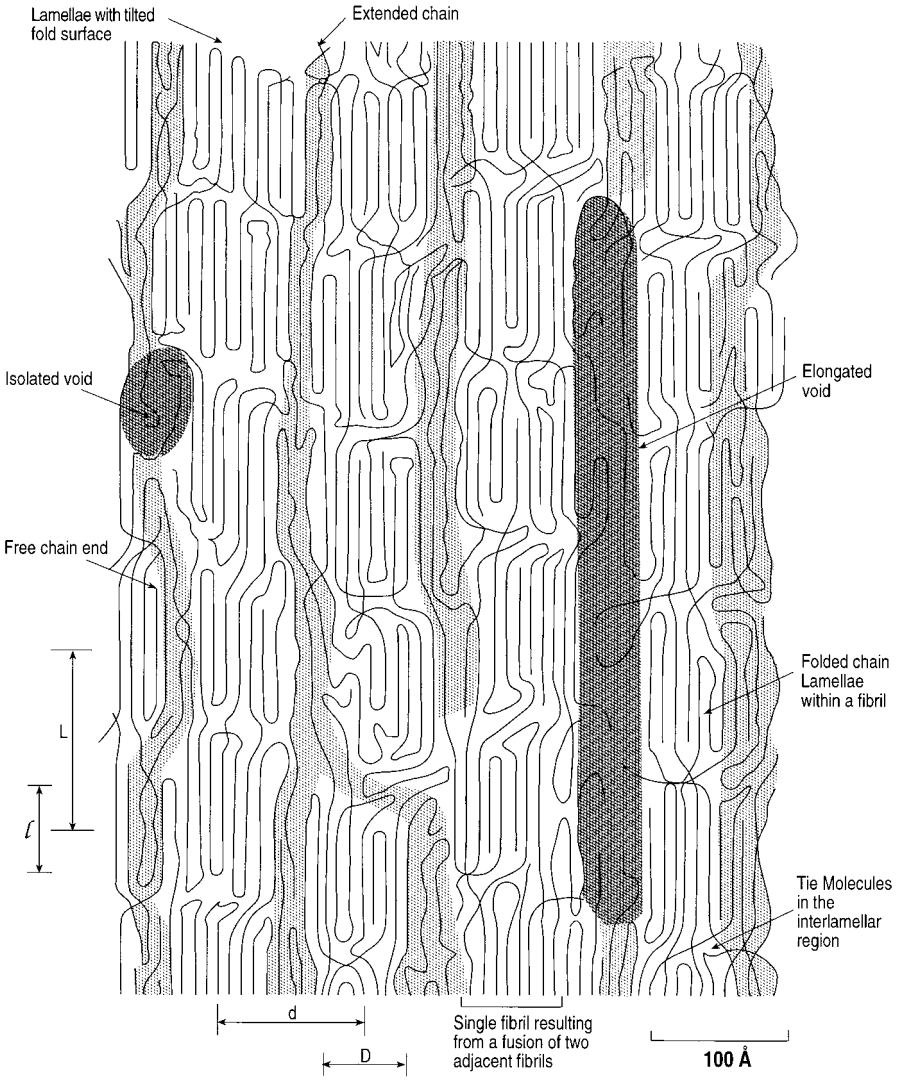

Figure 1 A model of the fiber to illustrate the various parameters used in this article.

where q is the scattering vector ($4\pi \sin \theta/\lambda$), θ is one-half the scattering angle, λ is the wavelength, q_M is the minor axis of the ellipse going through the lamellar reflection in q-space, and A is the distance between the foci of the elliptical coordinates chosen to describe the pattern. The height

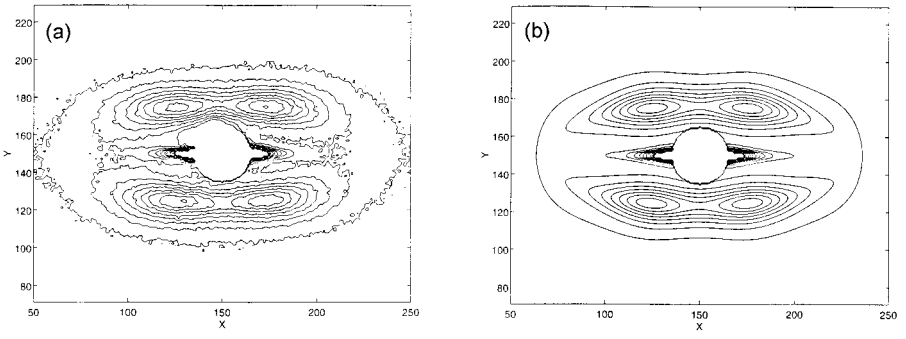

Figure 2 An example of the (a) observed and (b) fitted two-dimensional SAXS data from PET fibers (fiber T2).

of the lamellar stack is determined from the height of the lamellar reflection. The diameter D of the lamellae is obtained from the lateral width Δw (width perpendicular to the fiber axis) of the lamellar reflection using the expression

$$D = \lambda F / \sqrt{(\Delta w^2 - 0.56^2)} \quad (5)$$

where F is the sample to detector distance (743 mm), and 0.56 is the instrumental broadening in mm. Δw is azimuthal spread of the lamellar reflection and is calculated from the half-widths points ϕ_1 and ϕ_2, and is obtained from the elliptical-fitted parameters as follows:

$$\Delta w = \sqrt{(u^2 + A^2)} \int_{\phi 1}^{\phi 2} \sqrt{(1 - K \sin^2(\phi)} d\phi \quad (6)$$

$$K = A^2/(A^2 + u^2) \quad (7)$$

The interfibrillar spacing (d) was calculated as the Bragg spacing corresponding to the position of the interference peak in the equatorial streak. The length of the fibril (l_f) is determined from the u width of the equatorial streak.

RESULTS AND DISCUSSION

An example of the raw and the fitted two-dimensional data are shown in Figure 2. The three important features in the scattering patterns are the central diffuse scattering, the lamellar peak, and the fibrillar interference peak. These features are shown separately in the equatorial, longitudinal, and azimuthal scans given in Figure 3. Each of these peaks are characterized by their amplitude, width, and position. Figure 4(a) shows an example of the plot of the intensity maxima in longitudinal scans, such as the one shown in Figure 3(b), as a function of the scattering angle along the equator. The two traces correspond to the upper and lower halves of the SAXS pattern. The elliptical shape of such traces was analyzed by plotting L_ϕ^2 as a function of $\tan^2\phi$ [equation (2)]. These plots are shown for all of the fibers in Figure 4(b). The lamellar spacing (L_M or L) was calculated from the intercept, and the extension ratio (R) was calculated from the ratio of intercept to slope. Figure 4(c) shows the extension ratio of the lamellae increases with lamellar spacing.

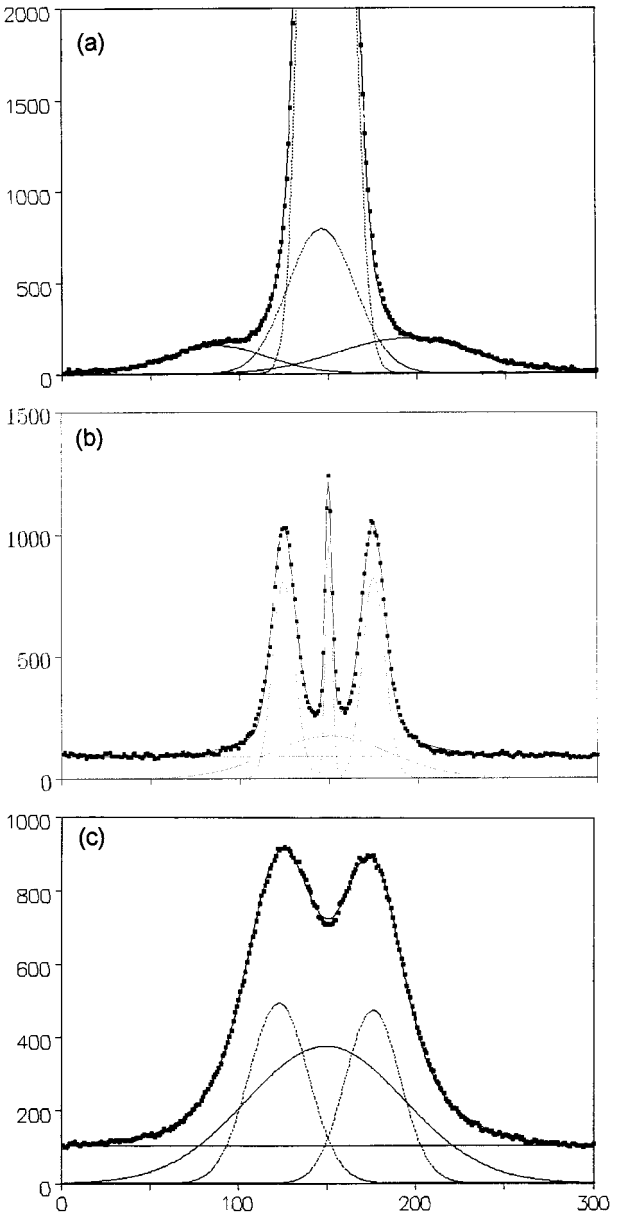

Figure 3 One-dimensional slices of the data shown in Figure 2. (a) Equatorial. (b) Meridional. (c) Azimuthal.

Data were also analyzed to obtain the additional parameters by a two-dimensional fit to the data in elliptical coordinates. The two parameters that are common to this two-dimensional fit and the above one-dimensional analysis—the lamellar spacing and the ellipticity—were found to be in good agreement. The complete results of the two-dimensional analysis are tabulated in Table I, and are plotted as a function of the shrinkage, tenacity, ultimate elongation, and modulus (LASE 5) in Figures 5–8. Correlation between the

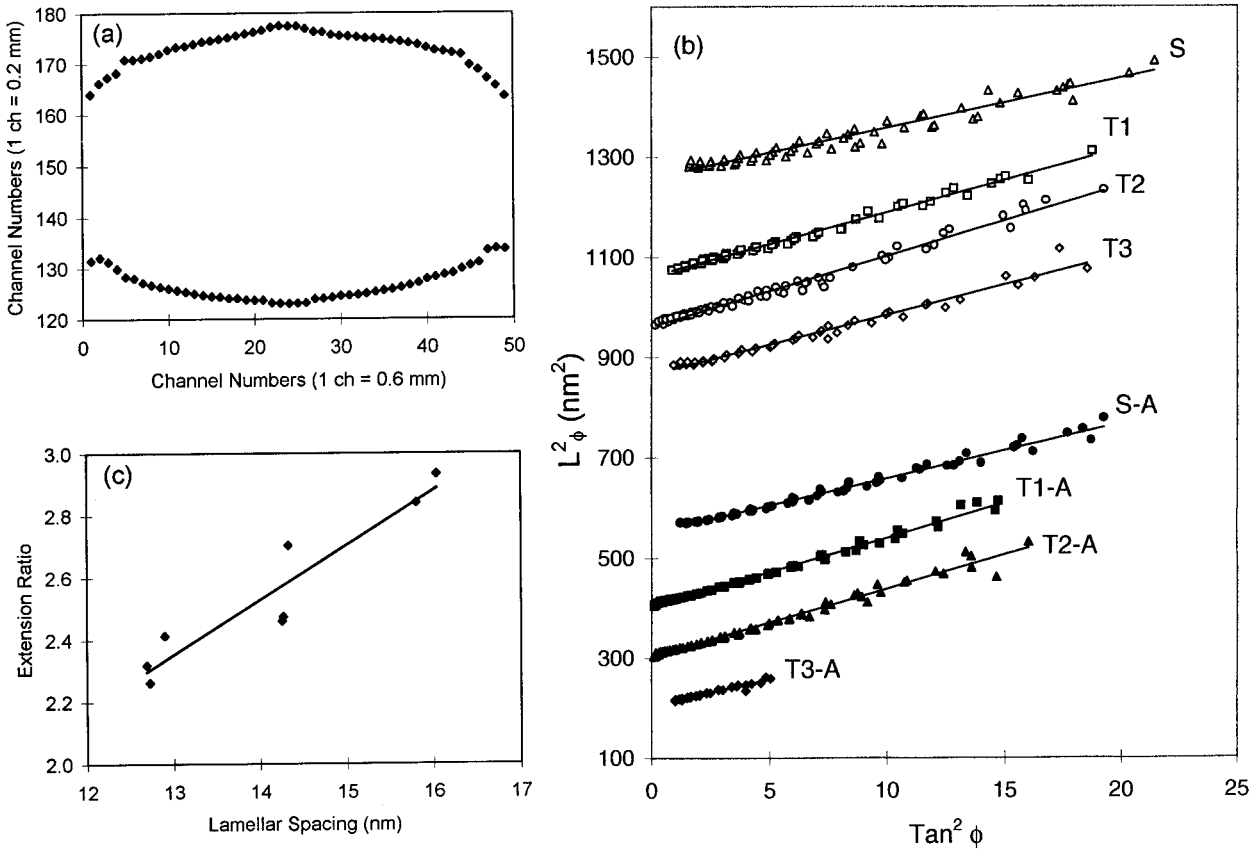

Figure 4 (a) Variation in the longitudinal position of the intensity maxima in the lamellar reflection as a function of the scattering angle along the equator for the fiber shown in Figure 2. ch = channel. (b) Plot of L^2_ϕ as a function of $\tan^2_\phi$. Open symbols in the top half refer to the as-received fibers, and the filled symbols in the bottom half refer to the heat-treated fibers. The curves have been offset for clarity. T3-A by 0, T2-A by 100, T1-A by 200, S-A by 300, T3 by 700, T2 by 800, T1 by 900, and S by 1000. (c) Variation in the extension ratio with long spacing; the parameters are calculated from the plots in (b).

various structural parameters and the mechanical properties are summarized in Table II.

The intensities from the various fibers were not normalized beyond collecting the data for about the same mass of fiber and for the same monitor counts. Thus, the small changes in *lamellar intensity* (I_l) and the *intensity of the central diffuse scattering* (I_d) within the two sets of fibers—the untreated and annealed—are not meaningful. However, I_l increased by a factor of 2 upon annealing. The I_d also increased upon heat treatment. I_d depends on the contrast between the fibrils and the interfibrillar amorphous regions that also have voids, and the volume fraction of the fibrils. The increase in I_d upon heat treatments suggests formation of new voids.

The *lamellar spacing* is highest in S. The long spacing increases by ~ 15 Å upon annealing the T fibers (14% in T1, 12% in T2, and 9% in T3), but decreases slightly in S. The *coherence length* (h_L) is low in S and T1 and high in T2 and T3 (i.e., decreases upon drawing), and increases upon annealing. The h_L in the three heat-treated T-h fibers is about the same, and is higher than in heat-treated S-h fibers (280 Å *vs.* 260 Å). The *diameter of the lamellae* (i.e., the fibrils) increases upon annealing and drawing thins the fibrils (draw ratios: S > T1 > T2 > T3). The *tilt angle* (ϕ) is lower in T fibers than in S fibers. ϕ increases upon drawing and decreases upon annealing. The peak corresponding to the *interfibrillar spacing* (d) was not clearly defined in all of the fibers. In the two fibers where this was distinguishable, the spacings were 48 Å in T1 and 63 Å in T2. The interfibrillar spacing increases by ~ 20 Å upon annealing (Table I). The length of the fibrils as

Table I Mechanical Properties and Structural Parameters of the Poly (ethylene terephthalate) fibers discussed in the article

Processing Conditions			Properties				Structural Features				
							Lamellar Parameters			Fibrillsr Parameters	
Fiber	Spinning Speed	Draw Ratio	UE (%)	Tenacity (g/denier)	Shrinkage (%)	LASE 5 (g/denier)	Spacing (Å)	Stack Height (Å)	2ϕ (Degree)	Spacing (Å)	Diameter (Å)
S	L	H	13.55	8.58	12.30	2.96	160	178	113	~ 45	59
S-h			12.78	8.39	4.77	4.04	158	252	100	~ 55	67
S-h3%			15.64	7.94	2.23	2.71	155	230	97	~ 65	69
T1	M1	M2	9.65	8.18	10.97	3.85	125	180	105	48	62
T1-h			11.16	7.99	2.23	3.70	143	287	84	~ 70	72
T2	M2	M1	9.54	7.85	7.40	4.37	127	218	93	63	65
T2-h			10.28	7.93	2.33	4.42	143	279	76	~ 75	71
T2-h1%			10.93	7.84	1.80	3.94	141	287	77	~ 75	70
T3	H	L	9.66	6.85	5.00	4.40	132	221	73	None	64
T3-h			10.00	6.63	1.60	3.89	144	292	54	None	78

H > M1 > M2 > L

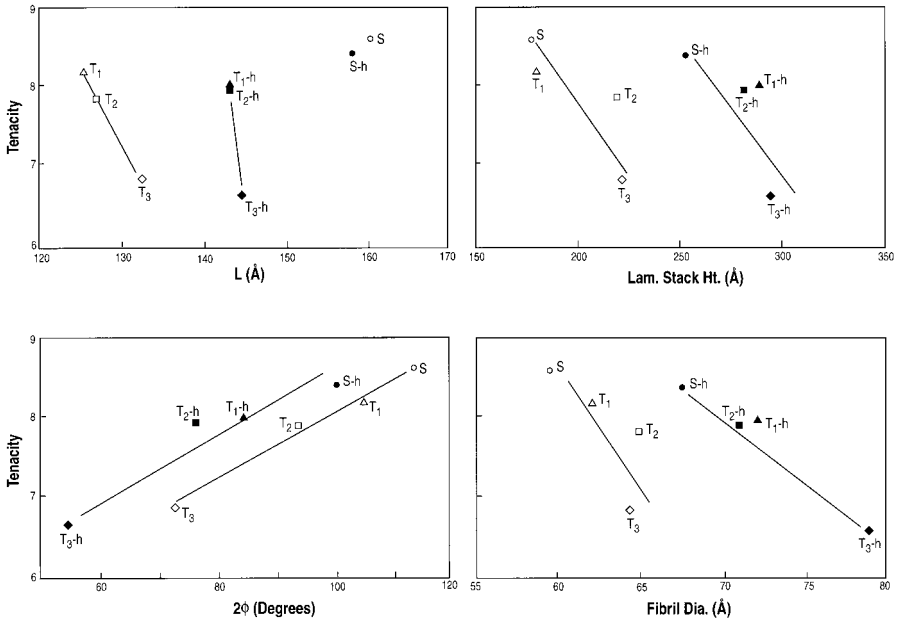

Figure 5 Tenacity *vs.* lamellar (Lam.) spacing, stack height (Ht.), fibril diameter (Dia.), and tilt angle. In this and the following three figures, the open symbols refer to the data from as-received (before annealing) fibers, and the filled symbols refer to the data from fibers after annealing. The annealed (heat-treated) fibers are also indicated by -h. Various shapes of the symbols describe the four fibers as follows: circle = S; triangle = T1; square = T2; diamond = T3.

calculated from the width of the diffuse equatorial scattering along the meridian was 2000–3000 Å.

The results in Figures 5(a), 6(a), 7, and 8 show that S is different from the T series of fibers. The S fiber has the highest tenacity, the largest shrinkage, the highest UE, and lowest LASE 5. Among the other three fibers, the trend is T1 > T2 > T3 in tenacity and shrinkage. Whereas the

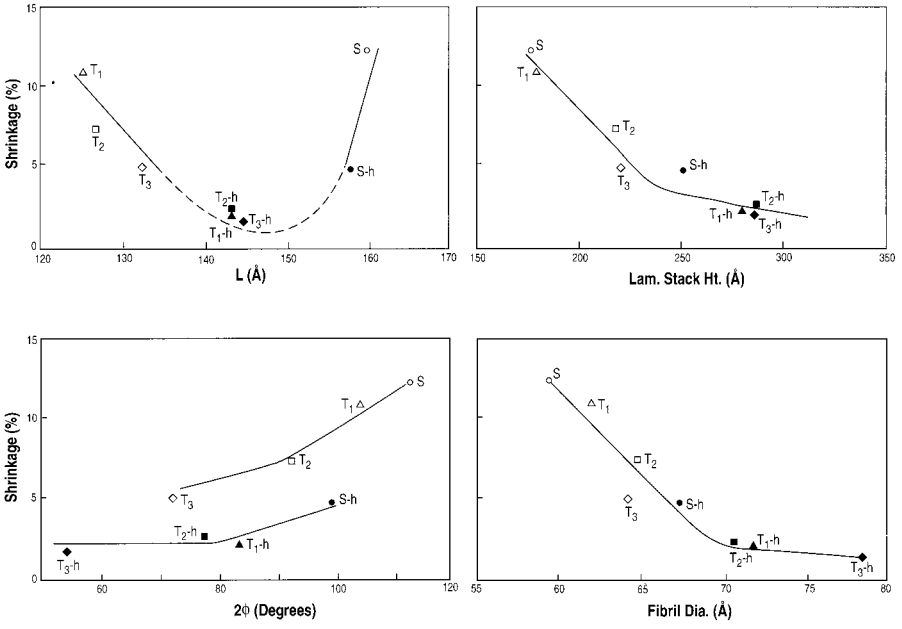

Figure 6 Shrinkage *vs.* lamellar (Lam.) spacing, stack height (Ht.), fibril diameter (Dia.), and tilt angle.

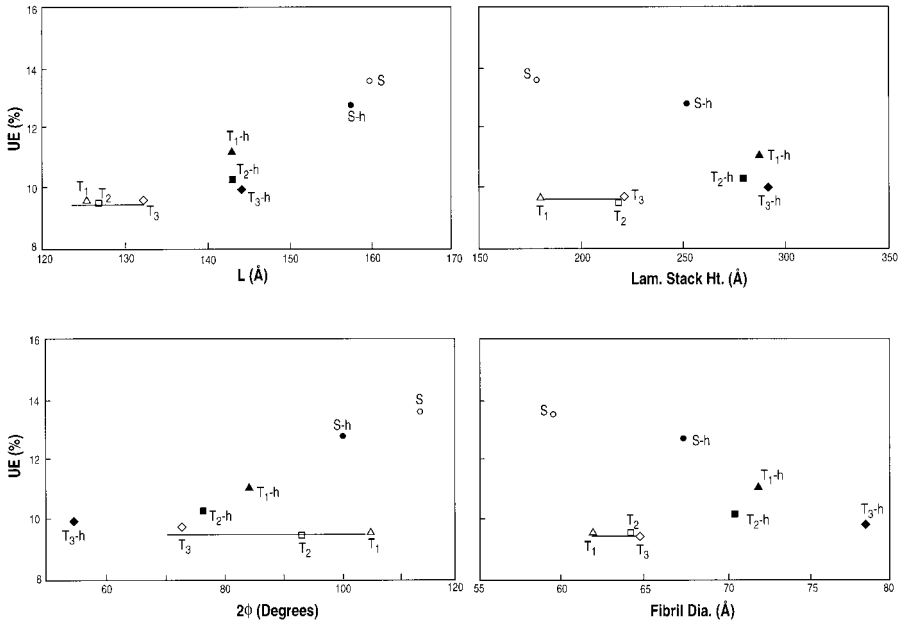

Figure 7 UE *vs.* lamellar (Lam.) spacing, stack height (Ht.), fibril diameter (Dia.), and tilt angle.

differences in tenacity remain after heat treatment, the differences in shrinkage are diminished, especially among the T fibers.

Figure 5 shows that, within the T series, the fibers with smaller lamellar spacing, shorter lamellar stacks, larger ϕ, and smaller diameter have a higher *tenacity*. Because the tenacity does not change significantly upon annealing, the relations between tenacity and L, h_L, ϕ, and D are preserved in the T-h fibers.

Figure 6 shows that, within the T fibers, smaller lamellar spacing appears to result in fi-

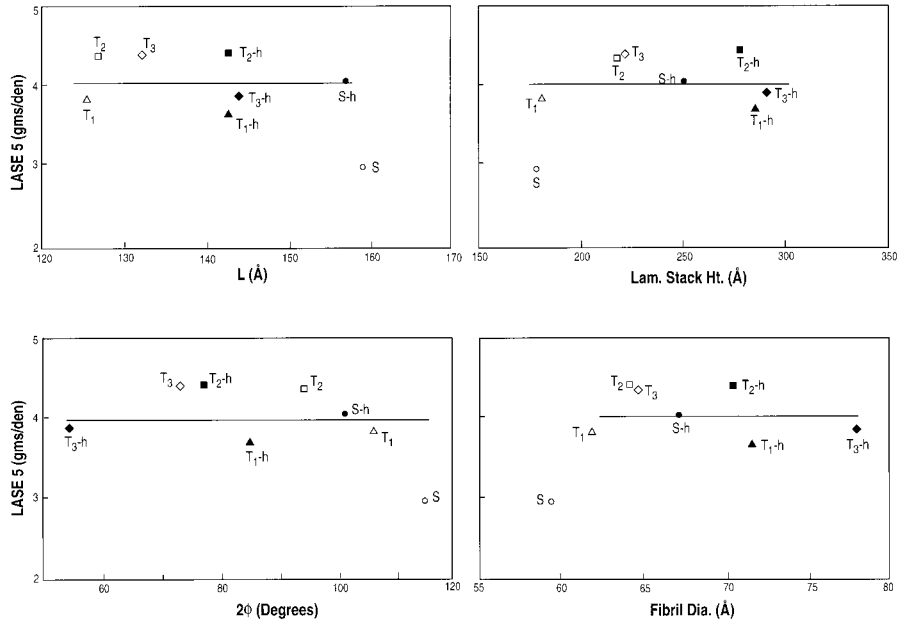

Figure 8 LASE 5 *vs.* lamellar (Lam.) spacing, stack height (Ht.), fibril diameter (Dia.), and tilt angle. den = denier.

Table II Correlation between Fiber Properties and Fiber Structure

	Tenacity (g/denier)		Shrinkage (%)			
	Before Annealing	After Annealing	Before Annealing	After Annealing	UE (%)	LASE 5 (g/denier)
Long spacing (L)	−0.999[a]	N	0.914		N	I[b]
Lamellar stack height (h_L)	−0.841	−0.731	−0.983		N	I[b]
Tilt angle (ϕ)	0.959	0.995	0.990	0.977	N	I[b]
Fibril diameter (D)	−0.772	−0.981	−0.967		N	I[b]

N = No obvious correlation between this parameter and property; I = property is independent of the structure.

[a] Excluding the S and S-h fibers.
[b] Excluding the S fiber.

bers with higher *shrinkage*. But, as evidenced by S fiber, large L does not guarantee lower shrinkage. Data also show that the fibers with smaller h_L (especially before heat treatment), larger ϕ, and smaller fibril diameter shrink more.

Figure 7 shows that *UE* in the three T fibers is about the same and is lower than in the S fiber. The UE increases in T fibers upon annealing and decreases in S, and the three T fibers become differentiated (T1-h > T2-h > T3-h). There is no obvious correlation between UE and ϕ, D, and h_L.

Figure 8 shows that fiber S has a lower *LASE 5* than all the other fibers; and, in these other fibers, LASE 5 is essentially independent of the various SAXS parameters previously discussed. The LASE 5 of the S fiber increases considerably upon annealing, remains the same in T1 and T2, and decreases in T3.

DISCUSSION

Although a combination of many structural characteristics gives rise to the desired properties, we will herein discuss the contribution of only those structural features derived from SAXS. *Lamellar spacing* (L) is the most widely used SAXS parameter. The increase in L is usually attributed to an increase in the thickness of the interlamellar amorphous phase and to the transformation of lamellae with smaller L by melting, followed by recrystallization into (or onto) lamellae with larger L. The relation between L and the extension ration R in Figure 4(c) suggests that the lamellae undergo an affine deformation, although the extension ratio of the lamellae is smaller than of the fiber as a whole. We find that the lamellar spacing measures but one aspect of the structure, and we describe herein other aspects in terms of coherence length (h_L), diameter of the lamellar stack (D), interfibrillar spacing (d), and tilt angle of the lamellar surface (ϕ).

Structural Parameters

The size of the lamellar stack can be characterized in terms of its height (h_L) and diameter (D). Although the diameter D of some of these fibers as determined by Tomlin and colleagues[9] follow the same order, their values are higher than ours by a factor of 2. Our values of D are comparable with the crystallite sizes in the equatorial plane, as determined from the $hk0$ reflection in wide-angle X-ray diffraction (62 Å in S, 56 Å in T1 and T2, and 60 Å in T3).[10] Interestingly, the fibril diameter is larger than the lateral crystallite size in the T fibers and is smaller in S. This difference between the wide-angle and small-angle sizes suggests that the distribution of the lateral sizes along the fiber axis in S and the T fibers are different, with a higher proportion of larger (and also with fewer defects) sizes being present in S than in T fibers. Because larger stack sizes in these fibers are not associated with any significantly higher crystallinity (unpublished data), it appears that there are fewer nucleation sites at higher crystallization temperatures on the spin line. This reduces the number of fibrils or the number of lamellar stacks within a fibril.

A parameter $L_\perp$, referred to as the interfibrillar spacing, is often calculated from the separation of the lamellar peaks perpendicular to the fiber axis in the 4-point patterns. In this model, these reflections are due to alignment of the lamellae in the adjacent fibrils in a fibrillar aggregate. Because the width of the lamellar

reflection is about the same as that of the lateral size of the crystals, as determined from the width of the wide-angle reflections, it is unlikely that lamellar reflections arise from an aggregate of fibrils. We prefer herein the alternative interpretation in which the lamellar reflections are off-axis because the fold surface of the lamellae is not perpendicular to the fiber axis, but makes an angle ϕ.[11,12]

The *tilt angle* ϕ appears to be an important structural characteristics of the fiber and is correlated to many of the properties of the fiber. As in other fibers, magnitude of ϕ increases upon drawing, and decreases with spinning speed and upon annealing. The fibers retain the memory of their tilt angle in the precursor fibers as evidenced by the approximately *constant decrease in* ϕ *after heat treatment.* Fibers in which the fold surface of the lamellae is perpendicular to the fiber axis shrink the least.

The *interfibrillar spacing* reflection clearly observed in the equatorial streak of the T1 and T2 fibers [Fig. 3(c)] suggests a fluid-like ordering of the fibrils in the equatorial plane in these fibers. Ordered fibrils were not observed during one-step crystallization that occurs during high-speed spinning (T3). A rather diffuse interfibrillar peak in the low speed spun but highly drawn S fiber. It is possible that distinct fibrillar aggregates are formed only during the drawing of fibers with low-to-moderate crystallinity. We find that fibers in which fibrillar aggregates are distinct have both high tenacity and high shrinkage. The interfibrillar spacing is not much greater than the fibril diameter, as would be expected from the presence of interfibrillar amorphous chain segments between the fibrils. It is possible that the diameter and the interfibrillar spacing represent different averages: diameter is measured by Scherrer broadening of the lamellar reflections, and spacing is measured by the Bragg peak in the equatorial streak. Alternatively, the larger diameter fibrils do not contribute to the interfibrillar spacing, especially in the heat-treated fibers, perhaps because of lack of contrast between the fibrils and the interfibrillar material in aggregates of fibrils of large diameter.

Mechanical Properties

In general, structural features such as smaller degree of amorphous orientation that reduce shrinkage also lower the tenacity. If this was the only parameter then, the dimensional stability can be improved only at the expense of tenacity, and both shrinkage and the tenacity can be improved only by changing the underlying relation between structure and performance [e.g., by changing the behavior of a polymer chain (a different polymer), by changing the interaction between the chains (mixture of two polymers), or between the crystalline and amorphous chains (change in processing, such as from melt spinning to gel spinning)]. However, the effect of heat treatment (Figures 5 and 6) shows that it is possible to manipulate other aspects of the structure so as to affect the shrinkage while leaving the tenacity unchanged.

Tenacity is determined by the load-bearing ability of the amorphous chains between the fibrils and those between the lamellae within a fibril. For the same crystallinity, a smaller fraction of the oriented amorphous chains results in fewer chains in near-parallel alignment to carry the load. Because of the resulting higher stresses, they break at lower loads. Thus, lower tenacity in T3 could be due to a large fraction of unoriented amorphous chain segments resulting from fast crystallization at high-speed spinning. Structures with a larger fraction of oriented amorphous chains segments appears to be associated with small h_L, D, and L and large ϕ (i.e., shorter and thinner lamellar stacks with more oblique and closely spaced lamellar planes).

Shrinkage is essentially an entropic phenomena. Thus, a decrease in the fraction of the oriented amorphous chains reduce shrinkage. Shrinkage considerably below the melting point is a result of the loss of orientation (coiled rather than extended chain conformation) of the interfibrillar-oriented amorphous chain segments, including tie molecules.[2,3,13] Shrinkage of fibers exposed to temperatures higher than at which earlier crystallization took place is accompanied by crystallization of oriented amorphous chain segments or melting and recrystallization of poorly crystallized lamellae. Fibers with larger lamellar stack, both in diameter and height, and less oblique lamellar planes shrink less. Tomlin and colleagues[9] have noted a smaller amount of interfibrillar material in the dimensionally stable fibers. A larger amorphous domain in the interfibrillar regions increases the likelihood of free (nontie) molecules farther away from the surface, and thus to contribute to shrinkage. They also found higher interfibrillar amorphous compliance in the T fibers.

UE is determined by the competition between slippage and breakage of the chains, lamellae, or fibrils. Figure 7 shows that processing conditions that increase L also increase UE. High draw ratio in S fiber which gives rise to large L yields fibers with larger UE. Most interestingly, while increase in L in T fibers is accompanied by an increase in UE, a decrease in L in S fibers is accompanied by a decrease in UE. It is possible that UE depends on the amount of interlamellar amorphous chain segments. Higher lamellar intensity in the annealed fibers (because the crystal density in these fibers is essentially unchanged) suggests that there is indeed a decrease in the orientation and the density of packing in the interlamellar amorphous regions that could increase the UE.

LASE 5 is determined by the mobility or stiffness of the chain segments that respond to load at low elongations. The structural changes that affect tenacity, shrinkage, and UE do not seem to affect LASE 5. We speculate that rather than the parameters such as size and orientation of the crystalline and amorphous domains, the connectivity within the amorphous domains and between the amorphous and crystalline domains affects LASE 5. These linkages have to be active only at low elongation, and not at higher elongation at which the tenacity of the fiber is determined. It has been suggested that tenacity is affected by the interlamellar tie molecules and the LASE 5 by the interfibrillar tie segments.[9,14–16] Our data show only that the linkages that determine the tenacity do not change during heat treatments, and those that affect LASE 5 are sensitive to details of the spin-draw sequence (S or T). It is possible that the structrual features which determine LASE 5 are the same as those which affect UE and shrinkage, but distinct from those which affect tenacity.

LASE 5 does not change upon constrained annealing in T, but increases in S. A higher LASE 5 in the T fibers than in S suggests that the linkages or entanglements, such as the ones discussed in the previous paragraph, are already present in the T fibers. Orienting the melt at high speeds (T) seems to have the same effect on LASE 5 as constrained annealing of a highly drawn yarn (S). It is possible that, when the fibers are spun at high speeds—as the average orientation of the amorphous chains increases—the entanglements remain, and subsequent crystallization will freeze-in these entanglements because the crystallization occurs faster than the rate of molecular relaxation (T fibers).[17] In contrast, drawing after low-speed spinning will remove these entanglements or labile crosslinks (S fibers). This would account for the higher LASE 5 and lower UE in the T fibers.

In the S fiber with low LASE 5, a decrease in UE upon constrained annealing is associated with an increase in LASE 5. However, the S fiber relaxed 3% during heat treatment behaves similar to the T fibers (i.e., the UE increases, but LASE 5 does not change). Could it be that constrained annealing in S fiber produces taut tie molecules[18] or linkages between the lamellae across the interfibrillar regions, and this increases LASE 5 and reduces UE just as in high-speed spun fibers? When the S fibers are relaxed during heat treatment, the orientation of the amorphous segments decreases and as a result the UE increases; but, the number and the nature of the tie molecules are not affected and therefore LASE 5 remains unchanged.

The untreated S fiber, which is the only yarn drawn from unoriented precursor fiber, has a lower LASE 5 than all the other fibers, and differs from all the other fibers in having a longer L, higher ϕ, and smaller D. What is so different about the S fiber? It has a lower molecular weight. But this may not explain all the differences between T and S fibers. Whereas L increases upon annealing in T fibers, it decreases in S, which is unusual. Also unusual is that UE increases in T fibers, it decreases in S, whereas LASE 5 is unchanged in T and increases in S. These differences show that low crystallinity and low orientation in the precursor fiber generates very different connectivity between the amorphous and crystalline regions upon drawing in the S fibers, although the final crystallinities and orientations may be the same as in T. This gives rise to low LASE 5 in S, although the high strain modulus is the same as in T.

CONCLUSIONS

A detailed analysis of the lamellar structure can provide parameters that can be used to understand the structural features that either directly or indirectly influence the properties. Increase in the spinning speed results in large h_L, small ϕ, large D, and small d. Drawing an unoriented yarn (S fiber) gives large L, lower coherence length, large ϕ, and smaller fibril diameter. Upon heat treatment, the lamellar (long) spacing increases in T and is essentially unchanged in S;

the intensity of the lamellar peak increases; the height and the diameter of the lamellar stacks increases; the tilt angle ϕ and the interfibrillar spacing decrease; and the central diffuse scattering increases. The route to the final state of structure, crystallinity, and orientation, such as preorientation of the fibers, seems to cause subtle changes in the structure of otherwise similar fibers, and these bring about significant changes in the performance of the fibers.

REFERENCES

1. R. Huisman and H. M. Heuvel, *J. Appl. Polym. Sci.,* **37,** 595 (1989).
2. N. S. Murthy, S. T. Correale, and R. A. F. Moore, *J. Appl. Polym. Sci. Appl. Polym. Symp.,* **47,** 185 (1991).
3. N. S. Murthy, C. Bednarczyk, H. Minor, and S. Krimm, *Macromolecules,* **26,** 1712 (1993).
4. G. Wu, J.-D. Jiang, P. A. Tucker, and J. A. Cuculo, *J. Polym. Sci. Polym. Phys.,* **34,** 2035 (1996).
5. G. Wu, P. A. Tucker, and J. Cuculo, *Polymer,* **38,** 1091 (1997).
6. R. J. Matyi and B. Crist, Jr., *J. Macromol. Phys.,* **B16,** 15 (1979).
7. N. S. Murthy, D. T. Grubb, and K. Zero, Proceedings of the ACS Division of Polymeric Materials: Science and Engineering, **79,** 363 (August 1998).
8. N. S. Murthy, K. Zero, and D. T. Grubb, *Polymer,* **38,** 1021 (1997).
9. D. W. Tomlin, C. M. Roland, and L. I. Slutsker, *J. Polym. Sci. Polym. Phys.,* **31,** 1331 (1993).
10. Y. Fu, B. Annis, A. Boller, Y. Jin, and B. Wunderlich, *J. Polym. Sci. Polym. Phys.,* **32,** 2289 (1994).
11. D. D. Pope and A. Keller, *J. Polym. Sci. Polym. Phys. Ed.,* **13,** 533 (1975).
12. T. H. Gilman, M. R. Resetaritis, and B. Crist, Jr., *Polym. Eng. Sci.,* **78,** 477 (1978).
13. V. B. Gupta, *J. Text. Inst.,* **86,** 299 (1995).
14. K. L. Peng and C. M. Roland, *J. Polym. Sci. Polym. Phys.,* **31,** 1339 (1993).
15. N. S. Murthy, C. Bednarczyk, P. B. Rim, and C. J. Nelson, *J. Appl. Polym. Sci.,* **64,** 1363 (1997).
16. P. B. Rim and C. J. Nelson, *J. Appl. Polym. Sci.,* **42,** 1807 (1991).
17. R. M. Gohil, *J. Appl. Polym. Sci.,* **52,** 925 (1994).
18. D. R. Salem and H.-D. Weigmann, *J. Polym. Sci. Polym. Phys.,* **29,** 765 (1991).